Effect of the size distribution of magnetic nanoparticles on metastability in magnetization relaxation

Yoh Yamamoto and Kyungwha Park

Effect of the size distributions of magnetic nanoparticles on metastability in magnetization relaxation

Yoh Yamamoto and Kyungwha Park

Department of Physics, Virginia Tech, Blacksburg, Virginia, 24061

We theoretically examine metastability occurring in magnetization relaxation for magnetic nanoparticles with size distributions. An array of magnetic nanoparticles is simulated using a spin $S=1$ ferromagnetic Blume-Capel model on a square lattice. The particle size distributions give rise to distributions of magnetic anisotropy. Including the distributions, we perform kinetic Monte Carlo simulations of magnetization relaxation at low temperatures for the Blume-Capel model. We compute the average lifetime of the metastable state from the simulations and the absorbing Markov chains method in the low temperature limit. We also carry out similar simulations and calculations for a constant value of magnetic anisotropy for comparison. Our results suggest that the lifetime of the metastable state is determined by the smallest particle for a given system, and that the lifetime with size distributions obeys a modified Arrhenius-like law, where the energy barrier depends on even temperature and standard deviation of the distributions as well as magnetic field and magnetic anisotropy.

I. INTRODUCTION

Recent advances in nanotechnology have allowed synthesis of nanoscale magnetic particles or molecules in various forms, such as in solutions, adsorbed at surfaces, or as powder compacts [1–3]. This was motivated by their applications for magnetic storage media [4, 5], biosensors [6], and contrast agents in magnetic resonance imaging [7–9]. Ideally, for a given system, magnetic nanoparticles may have uniform particle sizes and shapes, and molecules may have identical ligand orientations. However, scanning electron microscopy (SEM), transmission electron microscopy (TEM) and x-ray diffraction (XRD) data on magnetic nanoparticles/molecules revealed significant distributions of particle sizes and shapes [1–3, 10–12] or distributions of molecular ligand orientations [13]. In addition, various permanent magnets consist of many nanoscale grains with different sizes and shapes [14].

Distributions of sizes, shapes, and ligand orientations greatly influence properties of magnetic nanoparticles and nanocrystalline magnets. Therefore, it is critical to understand their magnetic properties as functions of the distributions. Magnetic anisotropy for magnetic nanoparticles or molecules originates from coupling between orbital and spin angular momenta of electrons, spin-orbit coupling (SOC). Thus, those distributions induce distributions of magnetic anisotropy, more specifically, distributions of magnetic anisotropy barriers (magnetization reversal energies in zero field) and of magnetic easy axes. As a result, coercivity, a remnant field, and magnetization relaxation vary with particle size and shape and with ligand orientation. This yields direct consequences in their applications.

For magnetic nanoparticles or molecules, four types of interactions may be considered. If the separations between nanoparticles are small, exchange interactions between nearest neighboring particles can play an important role. This is applied to single-chain magnets [13] and nanograins of NdFeB magnets [14]. However, if nanoparticles are well separated from one another, magnetic dipolar interactions are dominant over exchange interactions [12, 15]. In both cases, a magnetic anisotropy energy caused by SOC can be greater than either exchange interactions or dipolar interactions, and so this energy must be taken into account. The magnetic anisotropy energy consists of separate contributions from volume and surface anisotropy. At last, an interaction between the magnetic moments of nanoparticles and an external magnetic field (referred to as the Zeeman energy) needs to be included.

In this work, we are interested in metastability occurring in magnetization relaxation at low temperatures for ferromagnetic nanoparticles with size distributions only. The size distributions may be realized as distributions of magnetic anisotropy barriers. It is scientifically interesting and technologically important to understand magnetization relaxation as a function of magnetic field, magnetic anisotropy, and the distributions of magnetic anisotropy barriers. Despite its importance, theoretical understanding of metastability in magnetization relaxation has been, so far, limited to the Ising model (where the magnetic anisotropy energy does not exist) [16–19].

We start with a spin $S = 1$ ferromagnetic Blume-Capel model on a square lattice with periodic boundary conditions, where exchange interactions are dominant over dipolar interactions. We consider the following two cases: (i) when a uniaxial magnetic anisotropy parameter is constant and (ii) when the parameter has square and Gaussian distributions. We examine the decay or the average lifetime of the metastable state for the Blume-Capel model without and with the distributions of magnetic anisotropy parameter, using kinetic Monte Carlo (KMC) simulations and the absorbing Markov chains (AMC) method [18, 20]. It is found that the decay of the metastable state is determined by the smallest

value of the magnetic anisotropy parameter, and that the behavior of the magnetization relaxation deviates from the well-known Arrhenius law due to the distributions. Our findings can be generalized to magnetic nanoparticles with much higher magnetic moments.

This work is organized as follows. In Sec. II, we present our model and background in metastability appearing in magnetization relaxation. In Sec. III, we describe our computational methods, KMC simulations and the AMC method. In Sec. IV, we discuss our calculated form and simulation data of the average lifetime of the metastable state for a constant value of the magnetic anisotropy parameter and for distributed parameters. In Sec.V, we make a brief conclusion.

II.   OUR MODEL AND BACKGROUND

A.   Blume-Capel Model

For simulations of an array of magnetic nanoparticles, we consider a spin $S = 1$ ferromagnetic Blume-Capel model on a square lattice [21, 22]. A spin Hamiltonian $\mathcal{H}$ for the Blume-Capel model has the form of

$$\mathcal{H} = -2J \sum_{\langle i,j \rangle} S_{iz} S_{jz} - H \sum_i S_{iz} - D \sum_i S_{iz}^2, \tag{1}$$

where S_{iz} is the z component of spin at a site i and the magnetic easy axis is along the z axis. If the eigenvalue of S_{iz} is denoted as M_{iz}, there are three possible values of M_{iz}, $+1$, 0, and -1, for a quantum spin $S = 1$ (in the case of $\hbar = 1$). We assume that a classical spin is assigned at each site with three possible states of M_{iz}=+1, 0, and -1. The first term of Eq. (1) represents exchange interactions between nearest neighboring spins at sites i and j with an exchange coupling constant J (> 0). All spins are counted only once in the summation over nearest neighbors. The second term corresponds to the Zeeman energy with a magnetic field H. The last term indicates a magnetic anisotropy energy with a uniaxial magnetic anisotropy parameter D (> 0). Here DS^2 equals the second-order perturbation energy when one treats SOC, $\lambda \vec{L} \cdot \vec{S}$, as a small perturbation [23], where λ is the SOC parameter. Since the magnetic easy axis is aligned along the z axis, the sites with $M_z = \pm 1$ have lower magnetic anisotropy energies than the sites with $M_z = 0$. We choose a spin $S = 1$ in the Blume-Capel model because this is the simplest case in which the magnetic anisotropy, or the third term, plays a non-trivial role. (For the Ising model, the third term does not contribute to the total energy.) We conjecture that the main effect of size distributions is to produce distributions of magnetic anisotropy barrier. Experiments on magnetic nanoparticles [24] support this hypothesis. Thus, the $S = 1$ Blume-Capel model can give rise to qualitative features relevant to experimental data. We use a square lattice of $L \times L$ with periodic boundary conditions. Henceforth, we use J as units of energy (or equivalently of H and D), while we use J/k_B as units of temperature, where k_B is the Boltzmann constant.

In the case of size distributions, larger particles may have higher magnetic anisotropy barriers than smaller particles. This can be viewed as larger particles having (i) either larger magnetic anisotropy parameters D with a fixed spin or magnetic moment per particle, (ii) or larger magnetic moments with the parameter D fixed. Within the Blume-Capel model, the former viewpoint is taken to consider the size distributions. Therefore, distributions of particle sizes are implemented as distributions of D. The third term of Eq. (1) is then replaced by $-\sum_i D_i S_{iz}^2$, where D_i is selected from distributions of D, in other words, different values of D are assigned at different sites.

Equilibrium ground-state spin configurations for the $S = 1$ Blume-Capel model (for a constant value of D) at zero temperature, are shown in Fig. 1, as a function of H and D [25]. For $(-D-4) < H$ and $H > 0$ (the region marked by $+\underline{1}$ in Fig. 1), the configuration with all sites having $M_z = 1$, is the ground state, while for $H < 0$ and $H < (D+4)$ (the region marked by $-\underline{1}$ in Fig. 1), the configuration with all sites having $M_z = -1$ has the lowest energy. For the rest of the region where $H < (-D-4)$ and $H > (D+4)$, the configuration with all sites having $M_z = 0$ is the ground state. The coexistence lines and the tricritical point are shown in Fig. 1. The critical temperature T_c for the Blume-Capel model at $D = 0$ was calculated using different methods: T_c=2.065 from the Bethe-lattice approximation [26] and 1.952 from the effective field theory [27]. The value of T_c at $H = 0$ increases as D increases. Monte Carlo simulations by Ref. [28] revealed that $T_c = 1.6950$ for $D = 0$ and 2.1855 for $D = 5$. Our previous Monte Carlo simulations showed that T_c =2.052 for $D = 4$ [29].

B.   Metastability in Magnetization Relaxation

Let us briefly review metastability occurring during the magnetization relaxation, in general (Fig. 2). Assume that a spin system is initially prepared with magnetization saturated along the positive z direction. This can be realized by
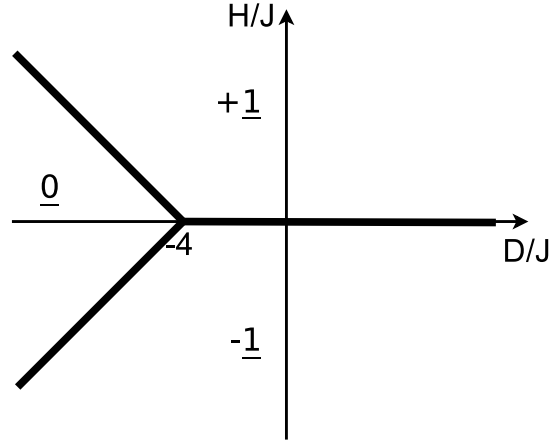
FIG. 1: The ground-state spin configurations for the $S = 1$ ferromagnetic Blume-Capel model at zero temperature. For example, $+\underline{1}$ indicates the ground state where all sites have $M_z = +1$. The bold lines represent the region where two ground states coexist. The tricritical point is located at $D = -4J$ and $H = 0$. Modified from Ref. [25].
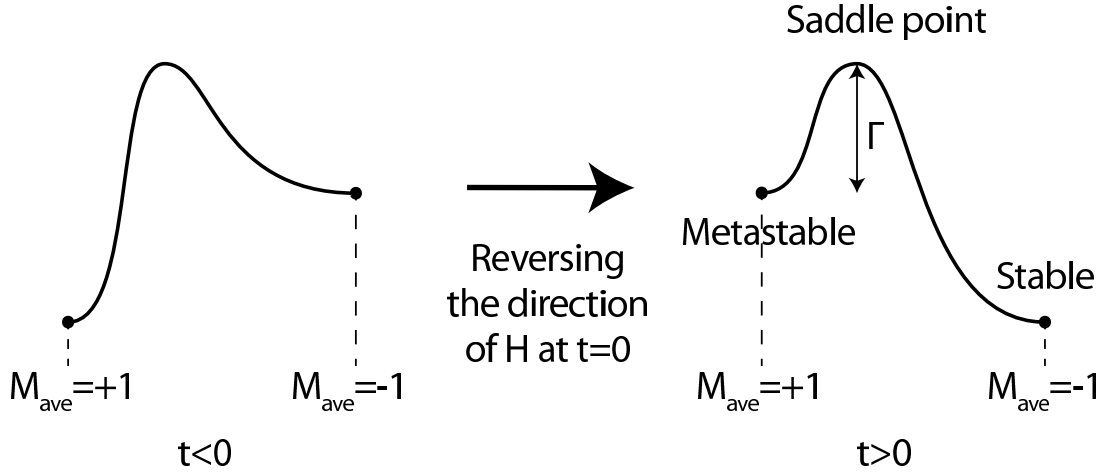

FIG. 2: A schematic diagram of metastability occurring during magnetization relaxation. The initial spin configuration consists of all sites with $M_z = +1$ ($t < 0$). After the reversal of the magnetic field, the initial configuration becomes metastable and the configuration with all sites having $M_z = -1$ is the ground state. Here Γ denotes an energy barrier to overcome for relaxation toward the ground state. The horizontal axis is the magnetization of the spin system.

applying a strong magnetic field along the positive z direction. Suppose that at $t = 0$ the magnetic field is reversed. Then at $t > 0$ the initial state now becomes a metastable state, while the state with all spins along the negative z direction is the ground state, as illustrated in Fig. 2. If a thermal energy is much lower than an energy barrier Γ, the system will stay in the metastable state for a while before overcoming the energy barrier to transit to the ground state. The time for which the system remains in the metastable state is referred to as lifetime of the metastable state. The relaxation rate of magnetization increases as T or $|H|$ increases. Thus, the lifetime of the metastable state depends on T and $|H|$.

We first summarize decay mechanisms of the metastable state for the Ising model since they can be applied to the Blume-Capel model. The decay mechanisms for the Ising model with periodic boundary conditions were studied using the droplet theory [30] and Monte Carlo simulations by Refs. [16, 17]. Three decay regimes were proposed [16–18]. (i) In a strong-field regime, the magnetic field is so strong that the metastable state is short-lived ($R_c < a$), where a is the lattice spacing and R_c is the radius of the critical droplet. (ii) In a multi-droplet (MD) regime, more than one supercritical droplet can be accommodated, and those droplets grow during the decay ($a \ll R_c < R_0 \ll L$), where R_0 is the mean droplet separation. (iii) In a single-droplet (SD) regime, the decay is driven by a single critical droplet ($a < R_c \ll L \ll R_0$). As shown in Refs. [16–18], for a given lattice size L, at substantially low temperatures, the Ising model is in the SD regime for $|H| < 4$.

Let us now discuss some basic features of the decay of the metastable state for the Blume-Capel model when D is
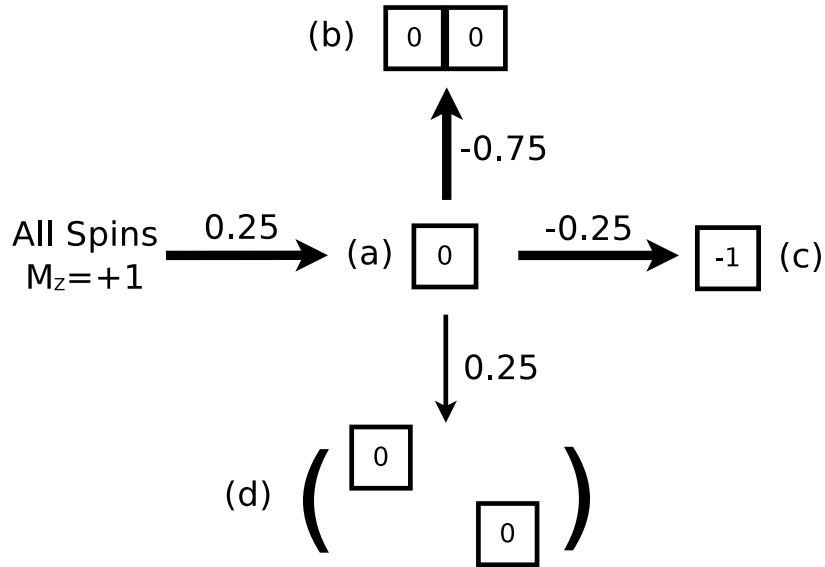
FIG. 3: A schematic diagram of a few initial paths and corresponding spin configurations for the magnetization relaxation for the Blume-Capel model at $H = -4$ and $D = 0.25$. In the initial configuration all sites have $M_z = +1$. A square containing a number M_0 represents a single flipped spin with $M_z = M_0$ from the initial configuration. The critical droplet is formed in the configuration (a). For the configuration (b), the two sites with $M_z = 0$ are nearest neighbors, while for the configuration (d), they are not nearest neighbors. The energy differences ΔE between two configurations are shown right next to the arrows. The bold arrows represent energetically favorable paths in the limit of $T \to 0$. Modified from Fig.4 of Ref. [29].

constant. (The case of distributions of D will be discussed in Sec.IV.B.) For simplicity, we, henceforth, focus on the SD regime which can be realized for $|H| < (D+4)$ in the low-temperature limit for a given lattice size L. More specifically, we use the parameter values of $H = -4$ and $D = 0.25$ throughout this study. As illustrated in Fig. 3, we first calculate energy differences between different spin configurations for several initial relaxation paths. Considering those energy differences, we conjecture energetically favorable paths for relaxation of magnetization, which are indicated by the bold arrows in Fig. 3. We find that the critical droplet consists of a single site with $M_z = 0$ (in the configuration (a) in Fig. 3). The energy barrier Γ is found to equal $(4 + D - |H|)$, which corresponds to the energy difference between the initial configuration and the configuration (a). More quantitative results using KMC simulations and the AMC method are presented in Sec.IV.

III.   COMPUTATIONAL METHODS

We present two methods to compute the average lifetime of the metastable state, $\langle \tau \rangle$, for the Blume-Capel model: (i) KMC simulations and (ii) the AMC method. As discussed in Refs. [29, 31], dynamics or transition rates between different spin configurations greatly affect the average lifetime of the metastable state. In rare cases, even the energy barrier Γ can change with underlying dynamics [31]. Therefore, it is desirable to use transition rates relevant to dynamic properties of the systems of concern. However, in this work, we are interested in understanding of the effect of distributions of D and so a choice of any convenient dynamic would be sufficient. We use the Glauber transition rates [32] where the spin-flip or transition probability p is given by

$$p = \frac{1}{1 + e^{\Delta E/T}} \tag{2}$$

where $k_B = 1$ and $\Delta E = E_{\text{new}} - E_{\text{old}}$. Here E_{old} (E_{new}) denotes an energy of the spin system before (after) a single spin flip.

Let us discuss the method for KMC simulations. For updates of spin configurations, one site is randomly selected out of the N $(= L^2)$ sites per Monte Carlo step. In the Blume-Capel model, a single spin flip corresponds to $\Delta M_z = \pm 1$. We use $L = 40$ (unless specified otherwise) and periodic boundary conditions. The average lifetime is defined to be the number of Monte Carlo steps until the total magnetization, $M_{\text{tot}} = \sum_{i=1}^{N} M_{iz}$, equals zero. In the SD regime, the standard deviation of the lifetime, $\Delta \tau$, is approximately of the same order of magnitude as $\langle \tau \rangle$ [16–18], that is, $\Delta \tau / \langle \tau \rangle \sim 1$. Thus, one needs to collect a large number of simulation sets for a thermally averaged lifetime at a given

temperature. We take a thermal average over 2000 escapes, where one escape implies one set of simulation runs until the initial configuration reaches to the state with $M_{\text{tot}} = 0$. We confirm that an increase in the number of escapes to 4000 does not change our simulation results with 2000 escapes. In the MD regime, $\Delta\tau$ is much smaller than $\langle\tau\rangle$. To examine if the system is in the SD or MD regime in the examined range of temperature for a given lattice size L, we compute $\Delta\tau/\langle\tau\rangle$ and monitor the average number of critical droplets during the 2000 escapes. For distributed values of D, in addition to the thermal average, we take an average over $10-100$ different representations of distributions for a particular value of standard deviation.

By analogy to the metastable decay for the Ising model [16, 17], the average lifetime of the metastable state for the Blume-Capel model is expected to increase exponentially with energy barrier at low temperatures. Thus, a large number of Monte Carlo steps are required to exit from the initial configuration and to reach to the configuration with $M_{\text{tot}} = 0$. For the constant value of D, we use advanced algorithms, the n-fold way algorithm [33] or the Monte Carlo with AMC (MCAMC) method [18, 20], to speed up the KMC simulations. These algorithms expedite the KMC simulations by categorizing all possible transitions into a finite number of spin classes, and by computing in advance the time to exit from the initial spin configuration or from a transient subspace. These algorithms are successfully implemented to the Blume-Capel model with the constant value of D. However, for distributions of D, the advanced algorithms may not be helpful anymore. The reason is that the value of D differs at different sites (determined by distributions of D), which prevents from setting spin classes with identical energies. In this case, a standard algorithm is used. For Gaussian distributions of D, a Box-Muller transformation [34] in a polar form is used to generate normally distributed random numbers.

Let us mention how to conjecture the analytical expression of $\langle\tau\rangle$, using the AMC method. For a given L, in the SD regime, once the critical droplet is formed, the time to reach to the configuration with $M_{\text{tot}} = 0$ is very short. So the average lifetime obtained from the KMC simulations can be approximated to the time to exit from a transient subspace in the AMC. For the $s = 2$ AMC method, we consider two transient states consisting of the initial configuration and the configuration (a), and three absorbing states comprising the configurations (b), (c), and (d) (Fig. 3). Using the transient and absorbing states, we create a transition matrix characterizing the AMC and find an analytical form of the exit time. In the limit of $T \to 0$, the simplified analytical form must be a good approximation to the average lifetime from the KMC simulations at low temperatures.

IV.   RESULTS AND DISCUSSION

We discuss the average lifetime of the metastable state for the Blume-Capel model at low temperatures when D is constant and when D has some distributions. In each case, we present the analytical expression of the lifetime in the limit of $T \to 0$ (using the AMC method) and the lifetime obtained from KMC simulations in units of Monte Carlo step. Even though we consider the particular parameter values of $H = -4$ and $D = 0.25$, our result is valid in the following regions: $(3 + D) < |H| < (4 + D)$ for $0 < D < 1/2$, and $(4 - D) < |H| < (4 + D)$ for $D \geq 1/2$. In these regions the critical droplet remains to be a single spin site with $M_z = 0$.

A.   Uniform Sizes: Constant Magnetic Anisotropy D

When the critical droplet is a single spin with $M_z = 0$, the exit time from the transient subspace is, using the $s = 2$ AMC method [18, 20] discussed earlier, given by

$$\langle\tau\rangle = \frac{8p_2 + p_{28} + p_{19} + (4L^2 - 10)p_1}{8p_2 + p_{28} + (2L^2 - 10)p_1}\frac{1}{p_1}, \tag{3}$$

$$p_1 = \frac{1}{1 + e^{(4+D-|H|)/T}}, \quad p_2 = \frac{1}{1 + e^{(3+D-|H|)/T}}, \tag{4}$$

$$p_{19} = \frac{1}{1 + e^{(-4-D+|H|)/T}}, \quad p_{28} = \frac{1}{1 + e^{(4-D-|H|)/T}}, \tag{5}$$

where p_1 is the Gaussian spin-flip probability from $M_z = 1$ to $M_z = 0$, when all the four nearest neighbors have $M_z = 1$. Here p_2 is the spin-flip probability from $M_z = 1$ to $M_z = 0$ when the sum of the four nearest neighboring moments equals $M_z = 3$, and p_{19} (p_{28}) is the spin-flip probability from $M_z = 0$ to $M_z = 1$ ($M_z = -1$) when the sum of the four nearest neighboring moments equals $M_z = 4$. Let us consider $0 < D < 1/2$. For $(4 - D) < |H| < (4 + D)$, in the limit of $T \to 0$, p_1 is approximated to $\exp[-(4 + D - |H|)/T]$, while p_2, p_{19}, and p_{28} approach unity. Thus, in the low-temperature limit, Eq. (3) becomes

$$\langle\tau\rangle = A/p_1 = Ae^{\Gamma(D,H)/T}, \qquad \Gamma(D, H) = 4 + D - |H|, \tag{6}$$
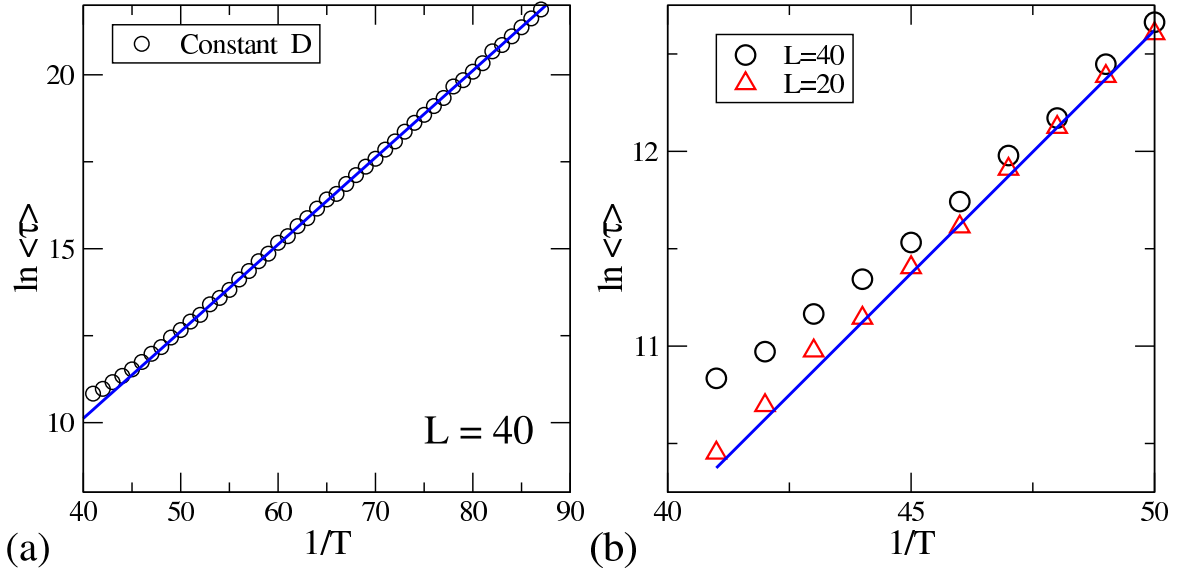
FIG. 4: (Color online) (a) The average lifetime $\langle \tau \rangle$ vs $1/T$ for the constant value of D for $L = 40$. The circles represent our simulation data, while the solid lines denote the fitting to Eq. (6). (b) Zoom-in of (a) at $1/T = 40 - 50$ with $L = 20$ and $L = 40$.

where the prefactor A is $10/9$ for $(4 - D) < |H| < (4 + D)$, while it is $9/8$ for $(3 + D) < |H| < (4 - D)$. This exit time obeys the Arrhenius law where the activation energy barrier Γ depends on D and H. Eq. (6) can be understood as follows. In the SD regime, at low temperatures, the exit time (or the lifetime of the metastable state) must be, approximately, inversely proportional to a probability of forming a critical droplet, p_{eq}. The probability p_{eq} equals p_1 when the critical droplet consists of a single spin with $M_z = 0$. Thus, $\langle \tau \rangle = A/p_{eq} = A/p_1$.

We perform KMC simulations using the n-fold way algorithm [33] for the parameter values of interest at $1/T = 41 - 90$ [Fig. 4(a)] for $L = 40$. At a given T, we take a thermal average over 2000 escapes. We fit the simulation data at $1/T = 55 - 90$ to a linear function, $\ln\langle\tau\rangle = \ln A + \Gamma/T$ (Fig. 4). As a result, we find that $\Gamma = 0.2497 \pm 0.0004$ and $A = 1.147 \pm 0.037$. Within the uncertainty, the simulated $\langle \tau \rangle$ agrees well with the exit time, Eq. (6), at $1/T \geq 55$. The simulation data below $1/T = 50$ with $L = 40$ are deviated from the linear function [Fig. 4(b)] because the system has not yet completely reached the SD regime. The temperature where the simulation data agree with the linear function (or the crossover between the SD and MD regimes) depends on L. Larger the lattice size is, lower temperature is needed for the agreement, which was shown for the Ising model [18]. Comparison between our simulation data with $L = 20$ and with $L = 40$ at $1/T = 40 - 50$ [Fig. 4(b)] corroborates this statement for the $S = 1$ Blume-Capel model.

B. Distributions of Magnetic Anisotropy D

Recent experiments showed that magnetic nanoparticles possess either Gaussian distributions f_G [3, 10, 14] or log-normal distributions f_{LN} of sizes [1, 11, 12]. For small variances, log-normal distributions look similar to Gaussian distributions. In this study, we consider only square and Gaussian distributions of D. Square distributions of D are chosen for their simplicity in analysis, which provides insight into the analysis for Gaussian distributions of D. Compared to log-normal distributions, Gaussian distributions are easier to implement in KMC simulations and to find closed analytical forms.

1. Square Distributions of D

We consider square distributions centered at $D_0 = 0.25$ with three values of width 2ε ($\varepsilon = 0.0125$, 0.025, and 0.0375). For a distribution of D, different values of D are assigned at different sites. As a result, a rate of transition between the initial configuration and the configuration (a) differs at different sites. Note that for the constant D, in the AMC, $p_{eq} = p_1$ when $(3 + D) < |H| < (4 + D)$ (for $0 < D < 1/2$). With a distribution of D, we predict that the probability p_{eq} can be written as the summation of the product of $p_{1,i}$ and $f(D_i)$ over all sites. $p_{1,i}$ defined to be p_1 for the site i, becomes $e^{-D_i/T}$ at $H = -4$ (in the limit of $T \to 0$). $f(D_i)$ is a probability density of selecting D_i from
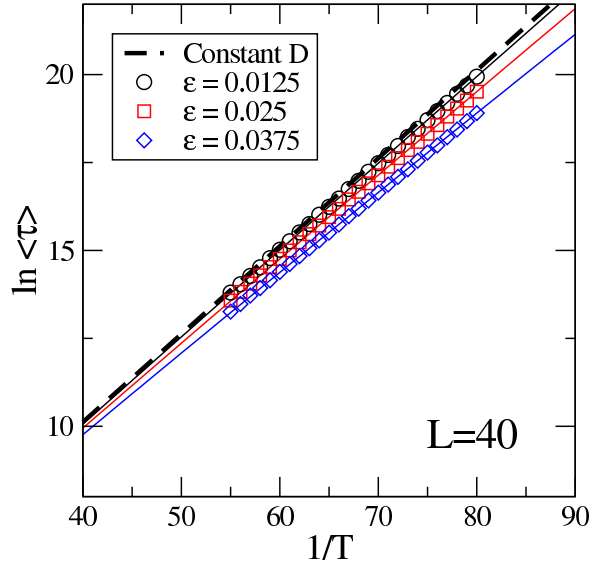
FIG. 5: (Color online) The average lifetime $\langle \tau \rangle$ vs $1/T$ for the square distributions of D centered at $D_0 = 0.25$ with the three widths of 2ε for $L = 40$. The symbols represent our simulation data, while the solid curves are obtained from the fitting (the second method) to Eq. (9) (Table I). For comparison, the fitting curve for the constant D (Fig. 4) is also included.

the distribution of D. After converting the summation into the integral over D, we obtain the probability p_{eq} as

$$p_{\mathrm{eq}} = \int f(D) e^{-D/T} \, dD \tag{7}$$

For the square distributions of concern, it can be written as

$$p_{\mathrm{eq}} = \frac{1}{2\varepsilon} \int_{D_0 - \varepsilon}^{D_0 + \varepsilon} e^{-D/T} \, dD. \tag{8}$$

Finally, the exit time or the average lifetime has the form of

$$\langle \tau \rangle = \frac{A}{p_{\mathrm{eq}}} = A \, \frac{\varepsilon/T}{\sinh \varepsilon/T} \, e^{D_0/T} \tag{9}$$

$$= \tilde{A}(T, \varepsilon) e^{\Gamma/T}, \tag{10}$$

where $A = 10/9$ from Sec.IV.A. In the low temperature limit, $\Gamma = D_0 - \varepsilon$ and $\tilde{A}(T, \varepsilon) = 2A\varepsilon/T$. Therefore, the energy barrier decreases linearly with increasing the width, and the prefactor $\tilde{A}$ now depends on both T and the width.

We perform KMC simulations for the square distributions of D with the three widths in the temperature range of $1/T = 55 - 80$ (Fig. 5). For computation of $\langle \tau \rangle$ at a given T and ε, we take a thermal average over 2000 escapes and an average over 10 square distributions. The average lifetime decreases with increasing the width (Fig. 5), as expected from Eq. (9). As the width increases, there are probabilities of selecting much lower values of D than D_0. The energy barrier is determined by the smallest value of D from the distributions. This lowers the energy barrier ($\Gamma = D_0 - \varepsilon$) and shortens the average lifetime. Regarding fitting of the simulation data, we use two different strategies: (i) the first strategy is to fit the data to Eq. (9) for D_0 and A with ε fixed, and (ii) the second method is to fit the data for A with D_0 and ε fixed. Using the first fitting method, we find that D_0 is 0.250 within the uncertainty of 0.001. The value of A bears one order of magnitude higher uncertainty (than that of Γ) and it significantly varies with the width: $A = 1.165 \pm 0.017$, 1.170 ± 0.017, and 1.212 ± 0.018, for $\varepsilon = 0.0125$, 0.025, and 0.0375, respectively. Using the second method, we find that the value of A is much closer to the predicted value, $10/9$, and that it is independent of the width (Table I). The fitting using the second strategy is shown in Fig. 5. As shown in Fig. 5, the simulation data agree well with the calculated lifetimes using Eq. (9).

2. Gaussian or Normal Distributions of D

We consider Gaussian distributions of D centered at $D_0 = 0.25$ with three values of standard deviation σ_D ($\sigma_D = 0.0125$, 0.025, and 0.0375). Similarly to the square distributions of D, we calculate the exit time from the transient
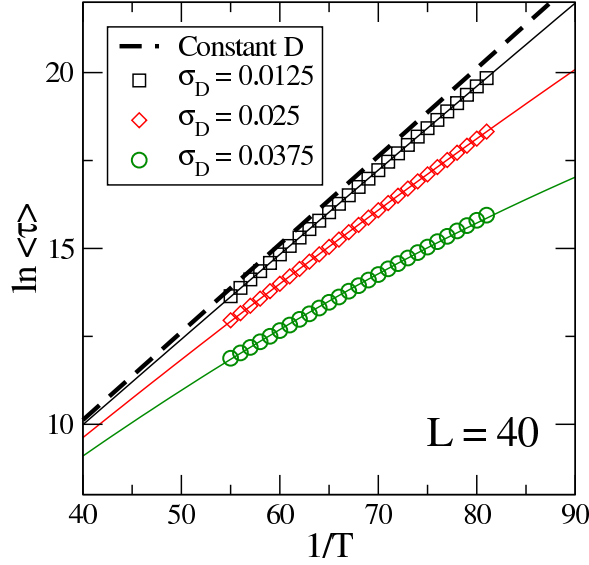
FIG. 6: (Color online) The average lifetime $\langle\tau\rangle$ vs $1/T$ for the Gaussian distributions of D centered at D_0 with the three standard deviations σ_D for $L = 40$. The symbols show our simulation data and the solid curves are obtained from the fitting to Eq. (11) (Table I). The fitting curve for the constant D is included.

subspace (in the AMC) using the probability p_{eq}, Eq. (7), where $f(D) = f_{\text{G}}(D)$. The exit time or the average lifetime has the form of

$$\langle\tau\rangle \;=\; A\exp\left(\frac{D_0}{T} - \frac{\sigma_D^2}{2T^2}\right) \tag{11}$$

$$=\; A\exp\left\{\Gamma(T, D_0, \sigma_D)/T\right\}. \tag{12}$$

Interestingly, in this case, the energy barrier Γ depends on T as well as D_0 and σ_D, which deviates from the Arrhenius law.

We perform KMC simulations for the Gaussian distributions of D with the three different standard deviations in the temperature range of $1/T = 55 - 81$ (Fig. 6). For computation of $\langle\tau\rangle$ at a given T and σ_D, we take a thermal average over 2000 escapes and an average over 100 Gaussian distributions. As expected from Eq. (11), the average lifetime decreases with increasing σ_D. The energy barrier decreases more rapidly with increasing σ_D than that for the square distributions (Fig. 5 vs Fig. 6). Using the similar argument to Sec.IV.B.1, the decrease in the barrier arises from the values of D selected from the lower end of the Gaussian distributions. For fitting of the simulation data, we use constrained fitting to Eq. (11) with D_0 and σ_D fixed, where A is the only free parameter. The result is listed in Table I. The value of A is close to $10/9$, even though it varies slightly with the value of σ_D. Its uncertainty increases with increasing σ_D. As shown in Fig. 6, the simulated data agree well with the calculated lifetimes (the fitting curves), for the distributions with small standard deviations such as σ_D=0.0125 and 0.025 (σ_D/D_0=5 and 10 %). However, in the case of $\sigma_D = 0.0375$ ($\sigma_D/D_0 = 15\%$), we observe noticeable deviations of the simulation data from the fitting curve, as temperature decreases (especially near $1/T = 80$ in Fig. 6). For clarification of these deviations, we plot differences between the simulated lifetimes and the fitting curves as a function of T for the constant value of D and the Gaussian distribution with $\sigma_D = 0.0375$ (Fig. 7). In the range of the temperature where the fitting is done, $1/T = 55 - 80$, the difference is almost zero for the constant D, while it starts to increase above $1/T = 70$ and reaches approximately to 0.1 at $1/T = 80$ for the Gaussian distribution. This is the reason that the value of A for $\sigma_D = 0.0375$ somewhat differs from that for $\sigma_D = 0.0125$ and 0.025.

Let us now discuss what causes the discrepancy between the simulated and calculated lifetime for $\sigma_D = 0.0375$ at low temperatures. One possibility is a finite size effect. For a finite lattice we can write Eq. (7) as $p_{\text{eq}} = (\sum_{i=1}^{N} e^{-D_i/T})/N$, where D_i is taken from the Gaussian distribution with $\sigma_D = 0.0375$. Using $\langle\tau\rangle = A/p_{eq}$, the average lifetime for the finite lattice becomes

$$\langle\tau\rangle = A\left(\frac{1}{N}\sum_{i=1}^{N} e^{-D_i/T}\right)^{-1}, \tag{13}$$

where $A = 10/9$. We generate the lifetime as a function of T, using both Eqs. (11) and (13), for two lattice sizes,
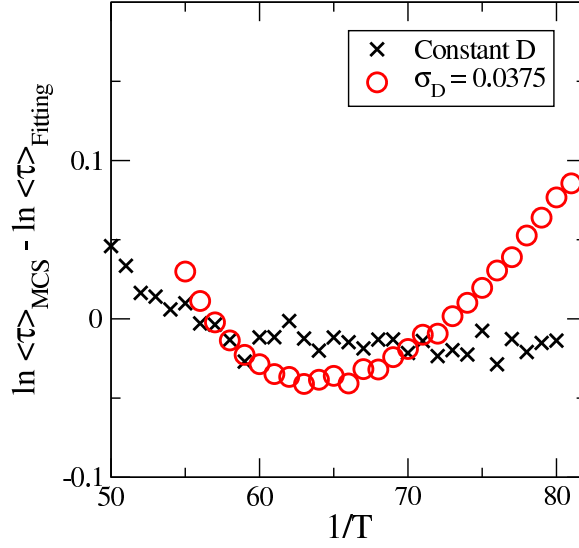
FIG. 7: (Color online) The differences between the lifetimes from the simulations and the fitting for the constant D and the Gaussian distribution with $\sigma_D = 0.0375$ for $L = 40$.
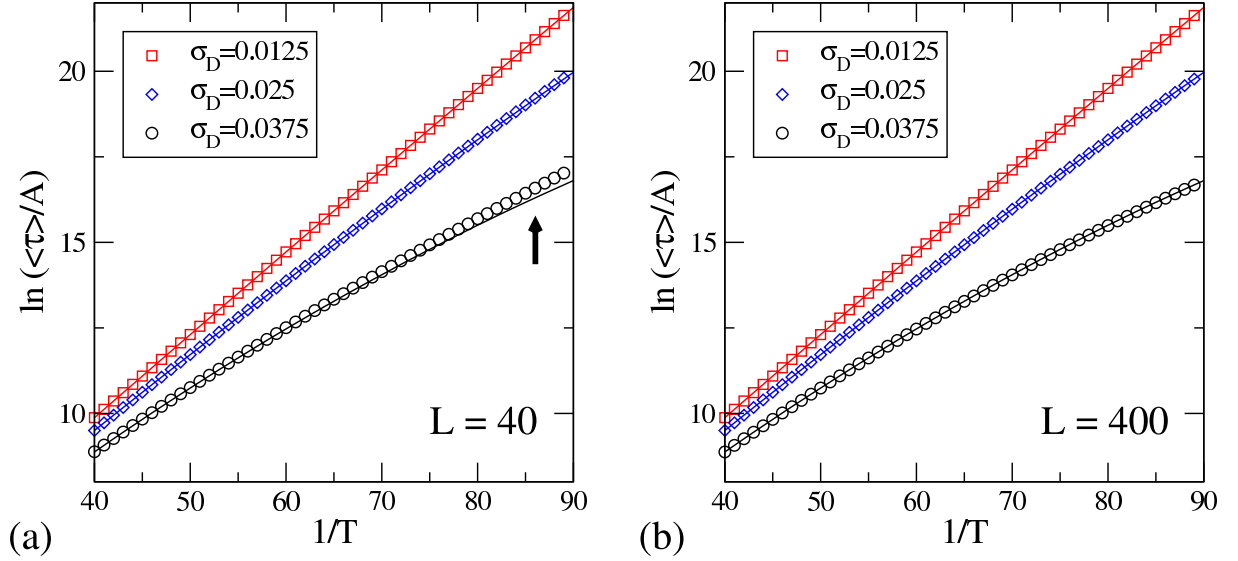

FIG. 8: (Color online) The calculated values of $\ln(\langle\tau\rangle/A)$ vs $1/T$ using Eq. (11) (symbols) and Eq. (13) (curves) for (a) $L = 40$ and (b) $L = 400$. For the curves, an average of 100 distributions is taken. The bold arrow in (a) emphasizes the region where the deviations between the symbols and the curve are substantial.

$L = 40$ and $L = 400$, as shown in Fig. 8. For proper comparison, when Eq. (13) is used, an average of 100 Gaussian distributions are taken for $L = 40$ and $L = 400$ (Fig. 8). As shown in Fig. 8 (a), for $L = 40$, in the case of $\sigma_D=0.0125$ and 0.025, the symbols agree well with the curves. This implies that there is no finite size effect for small values of σ_D for $L = 40$. However, for $L = 40$ and $\sigma_D = 0.0375$, the deviations between the curve and the symbols start to appear near $1/T = 65$ and they becomes more significant at lower temperatures [marked by the bold arrow in Fig. 8 (a)]. No such deviations are found for $L = 400$ and $\sigma_D = 0.0375$, as shown in Fig. 8 (b). This result corroborates that the deviations observed in Fig. 7 are caused by the finite size effect. It also suggests that the finite size effect must be considered in the analysis when the distributions are wide.

V. CONCLUSION

We have investigated the metastability in magnetization relaxation at low temperatures for magnetic nanoparticles with identical particle sizes and with non-uniform size distributions. For simulations of magnetic nanoparticles, we have used the $S = 1$ ferromagnetic Blume-Capel model on a square lattice without and with distributions of magnetic anisotropy. We have applied the AMC method and performed the KMC simulations on the Blume-Capel model in the SD regime ($H = -4$, $D = 0.25$, and $L = 40$), and computed the average lifetime of the metastable state at low temperatures. Our results are valid in the region $(3+D) < |H| < (4+D)$ for $0 < D < 1/2$ and $(4-D) < |H| < (4+D)$ for $D \geq 1/2$.

For nanoparticles with identical sizes, the energy barrier depends on magnetic field and magnetic anisotropy and so does the magnetization relaxation. Therefore, the average lifetime of the metastable state obeys the Arrhenius law. However, for nanoparticles with distributions of magnetic anisotropy, the energy barrier has the additional dependence on temperature and standard deviation of the distributions. Consequently, the lifetime obeys the modified Arrhenius-like law, and types of distribution functions determine the specific dependence of the energy barrier and prefactor of the lifetime on physical variables. The average lifetime was found to be shorter than that for the constant D, when the constant value of D coincides with the mean value of D in distributions. The lifetime decreases significantly as the width or the standard deviation of the distributions increases. This is because the average lifetime is determined by the smallest nanoparticle for a given system. We have also shown an importance of inclusion of the finite size effect when the distributions of magnetic anisotropy are wide. The features found in this study qualitatively agree with experimental data [1, 10, 11, 14, 24]. However, more quantitative comparison with experimental data, requires consideration of other factors which are beyond the scope of this work. A few examples of those factors are open boundary conditions, inclusion of the MD regime, distributions of shapes or magnetic easy axes, and consideration of dipolar interactions.

Acknowledgments

[1] M. A. Willard, L. K. Kurihara, E. E. Carpenter, S. Calvin, and V. G. Harris, Intl. Mat. Rev. **49**, 125 (2004).
[2] S. B. Choe and S. C. Shin, Phys. Rev. B **65**, 224424 (2002); M. Y. Im, D. H. Kim, and S. C. Shin, Phys. Rev. B **72**, 132416 (2005).
[3] R. Belhi, A. Adanlété Adjanoh, J. Vogel, M. Ayadi, and K. Adbelmoula, J. Appl. Phys. **108**, 093924 (2010).
[4] S. Sun, C. B. Murray, D. Weller, L. Folks, and A. Moser, Science **287**, 1989 (2000).
[5] S. H. Sun, Adv. Mat. **18**, 393 (2006); B. D. Terris and T. Thomson, J. Phys. D-Appl. Phys. **38**, R199 (2005).
[6] M. M. Miller, G. A. Prinz, S. F. Cheng, and S. Bounnak, Appl. Phys. Lett. **81**, 2211 (2002).
[7] A. K. Gupta and M. Gupta, Biomat. **26**, 3995 (2005).
[8] Y. L. Wang, W. Li, S. Y. Zhou, D. L. Kong, H. S. Yang, and L. X. Wu, Chem. Comm. **47**, 3541 (2011).
[9] J. E. Mertzman, S. Kar, S. Lofland, T. Fleming, E. van Keuren, Y. Y. Tong, and S. L. Stoll, Chem. Comm. 788 (2009).
[10] I. Volkov, M. Chukharkin, O. Snigirev, A. Volkov, S. Tanaka, and C. Fourie, J. Nanopart. Res. **10**, 487 (2008).
[11] S.-P. Yu, Y.-H. Liu, A.-C. Sun, and J.-H. Hsu, J. Appl. Phys. **106**, 103905 (2009).
[12] O. Crisan, K. von Haeften, A. M. Ellis, and C. Binns, Nanotechnology, **19**, 505602 (2008).
[13] K. Bernot, J. Luzon, A. Caneschi, D. Gatteschi, R. Sessoli, L. Bogani, A. Vindigni, A. Rettori, and M. G. Pini, Phys. Rev. B **79**, 134419 (2009).
[14] Y. Sun, R. W. Gao, W. C. Feng, G. B. Han, G. Bai, and T. Liu, J. Mag. Mag. Mat. **306**, 108 (2006).
[15] J. M. Vargas, W. C. Nunes, L. M. Socolovsky, M. Knobel, and D. Zanchet, Phys. Rev. B **72**, 184428 (2005).
[16] P. A. Rikvold, H. Tomita, S. Miyashita, and S. W. Sides, Phys. Rev. E **49**, 5080 (1994).
[17] H. L. Richards, S. W. Sides, M. A. Novotny, and P. A. Rikvold, J. Mag. Mag. Mat. **150**, 37 (1995).
[18] M. A. Novotny, "A tutorial on advanced dynamic Monte Carlo methods for systems with discrete state spaces," *Annual Reviews of Computational Physics IX*, edited by D. Stauffer, (World Scientific, Singapore, 2001), pp.153-210; arXiv.org: cond-mat/0109182v1.
[19] V. A. Shneidman, J. Stat. Phys. **112**, 293 (2003).
[20] M. A. Novotny, Phys. Rev. Lett. **75**, 1424 (1995).
[21] M. Blume, Phys. Rev. **141**, 517 (1966).
[22] H. W. Capel, Physica (Amsterdam) **32**, 966 (1966).
[23] K. Yosida, *Theory of Magnetism*, (Springer-Verlag, Heidelberg, Germany 1996), Chapter 3.
[24] A. J. Rondinone, C. Liu, and Z. J. Zhang, J. Phys. Chem. **105**, 7967 (2001).

[25] E. N. M. Cirillo and E. Olivieri, J. Stat. Phys. **83**, 473 (1996).

[26] Y. Tanaka and N. Uryû, J. Phys. Soc. Japan **50**, 1140 (1981).

[27] H. Polat, Ü. Akinci, and Í. Sökmen, Phys. Stat. Sol. B **240**, 189 (2003).

[28] R. da Silva, N. A. Alves, and J.R. Drugowich de Felício, Phys. Rev. E **66**, 026130 (2002).

[29] K. Park, Phys. Rev. B **77**, 104420 (2008).

[30] A. N. Kolmogorov, Bull. Acad. Sci. USSR, Phys. Ser. **1**, 355 (1937); W. A. Johnson and R. F. Mehl, Trans. Am. Inst. Min. Metall. Pet. Eng. **135**, 416 (1939); M. Avrami, J. Chem. Phys. **7**, 1103 (1939); M. Avrami, J. Chem. Phys. **9**, 177 (1941).

[31] K. Park, P. A. Rikvold, G. M. Buendia, and M. A. Novotny, Phys. Rev. Lett. **92**, 015701 (2004).

[32] R. J. Glauber, J. Math. Phys. **4**, 294 (1963).

[33] A. B. Bortz, M. H. Kalos, and J. L. Lebowitz, J. Comput. Phys. **17**, 10 (1975).

[34] G. E. P. Box and M. E. Muller, Ann. Math. Stat. **29**, 610 (1958).

TABLE I: Fitting of the Monte Carlo simulation data for the square and Gaussian distributions of D with $D_0 = 0.25$ and ε or σ_D fixed. The fitting functions and the prefactor A are shown, where $x = 1/T$.

	Fitting function	A (ε, σ_D=0.0125)	A (ε, σ_D=0.025)	A (ε, σ_D=0.0375)
Square	$A \frac{\varepsilon x}{\sinh(\varepsilon x)} e^{D_0 x}$	1.112 ± 0.002	1.117 ± 0.002	1.117 ± 0.003
Gaussian	$A \exp\left(D_0 x - \frac{1}{2}\sigma_D^2 x^2\right)$	1.118 ± 0.001	1.128 ± 0.002	1.251 ± 0.009